

The Galactic Center Weather Forecast

M. Mościbrodzka^{1†}, H. Shiokawa², C. F. Gammie^{2,3}, J. C. Dolence⁴

¹ *Department of Physics and Astronomy, University of Nevada, 4505 South Maryland Parkway, Las Vegas, NV 89154*

² *Astronomy Department, University of Illinois, 1002 West Green Street, Urbana, IL 61801*

³ *Department of Physics, University of Illinois, 1110 West Green Street, Urbana, IL 61801*

⁴ *Department of Astrophysical Sciences, Princeton University, Peyton Hall, 4 Ivy Lane, Princeton, NJ 08544*

† `monikam@physics.unlv.edu`

ABSTRACT

In accretion-based models for Sgr A* the X-ray, infrared, and millimeter emission arise in a hot, geometrically thick accretion flow close to the black hole. The spectrum and size of the source depend on the black hole mass accretion rate \dot{M} . Since Gillessen et al. have recently discovered a cloud moving toward Sgr A* that will arrive in summer 2013, \dot{M} may increase from its present value \dot{M}_0 . We therefore reconsider the “best-bet” accretion model of Mościbrodzka et al., which is based on a general relativistic MHD flow model and fully relativistic radiative transfer, for a range of \dot{M} . We find that for modest increases in \dot{M} the characteristic ring of emission due to the photon orbit becomes brighter, more extended, and easier to detect by the planned Event Horizon Telescope submm VLBI experiment. If $\dot{M} \gtrsim 8\dot{M}_0$ this “silhouette” of the black hole will be hidden beneath the synchrotron photosphere at 230GHz, and for $\dot{M} \gtrsim 16\dot{M}_0$ the silhouette is hidden at 345GHz. We also find that for $\dot{M} > 2\dot{M}_0$ the near-horizon accretion flow becomes a persistent X-ray and mid-infrared source, and in the near-infrared Sgr A* will acquire a persistent component that is brighter than currently observed flares.

1. Introduction

The recent discovery of a cloud moving towards the Galactic Center (Gillessen et al. 2012) creates a potential opportunity for testing models of Sgr A*. The $> 3M_\oplus$ cloud will

interact strongly with gas near nominal pericenter at $r_p \simeq 300\text{AU} \simeq 8000GM/c^2$ ($M \equiv$ black hole mass), and may change the black hole accretion rate \dot{M} . Since the structure of the cloud and the surrounding medium are uncertain, possible outcomes range from very small changes in the accretion rate over timescales of decades to rapid, large changes in the accretion rate.

The dynamical timescale at r_p is $t_d = (r_p^3/(GM))^{1/2} = 0.5\text{yr}$, and the viscous timescale $t_{vis} = (\alpha\Omega)^{-1}(R/H)^2 \approx 100\text{yr} \gg t_{pHD}$, assuming $\alpha = 0.05$ and $H/R = 0.3$, i.e. a hot, radiatively inefficient accretion flow. After an initial transient phase while the flow circularizes—accompanied by transient emission—it is natural to think the flow will settle into a steady state. The settling timescale could be as little as a few t_d , and so the steady state may arrive as soon as mid-2014. If the resulting flow can be modeled as a steady disk, the excess mass will drain away on the viscous timescale, i.e. the source will remain bright well into the 22nd century. It is therefore interesting to ask how changes in \dot{M} will manifest themselves observationally.

Current observations of Sgr A* show $F_\nu = 0.5 - 1$ Jy at 1-50 GHz with a nearly flat spectral slope (Falcke et al. 1998); $F_\nu \sim \nu^{p=0.17-0.3}$. The spectral slope becomes flatter and variable at 230-690 GHz, with $p = -0.46 - 0.08$, Marrone 2006), which is commonly interpreted as signaling a transition from optically thick to optically thin synchrotron emission. The discovery of polarized emission (polarization fraction at level of a few per cent) at $\lambda = 1.3\text{mm}$ and subsequent measurement of Faraday rotation imply a model dependent limit $2 \times 10^{-7} > \dot{M} > 2 \times 10^{-9}M_\odot\text{yr}^{-1}$ in the inner accretion flow (Bower et al. 2005, Marrone et al. 2006). Sgr A* is resolved by VLBI at 1.3mm where interstellar scattering is comparable to the intrinsic source FWHM $37_{-10}^{+16}\mu\text{as}$ (Doeleman et al. 2008). This is smaller than the apparent diameter of the event horizon $\sim 55\mu\text{as}$. Sgr A* fluctuates rapidly in the near-infrared (NIR), with average $F_\nu \sim 1\text{mJy}$ (Dodds-Eden et al. 2011). It is not yet detected at mid-infrared (MIR) wavelengths ($\lambda \leq 8.6\mu\text{m}$, e.g. Schödel et al. 2011). In the X-ray Sgr A* exhibits flares with characteristic duration of order an hour and a duty cycle of order 5%. The upper limit for quiescent state X-ray emission is $\nu L_\nu < 2.4 \times 10^{33}\text{ergs}^{-1}$ (Baganoff et al. 2003). We are not aware of any secular trends in these observed properties of Sgr A*.

One model of Sgr A* that fits most observational constraints is our relativistic accretion model (Mościbrodzka et al. 2009), where submillimeter, IR, and X-ray emission arise in an optically thin, geometrically thick disk close to the event horizon; radio emission is assumed to arise nonthermally in a synchrotron photosphere at larger radius (Özel et al. 2000), but is not predicted by our model, which focuses on the inner parts of the accretion flow. The underlying flow model is a general relativistic magnetohydrodynamic (GRMHD) simulation

(Gammie et al. 2003, Noble et al. 2006, Shiokawa et al. 2011). The emerging radiation is calculated using Monte Carlo (Dolence et al. 2009) and ray-tracing schemes. The 1.3mm flux originates as Doppler boosted synchrotron emission from the approaching side of the disk between $\sim 10GM/c^2$ and the innermost stable circular orbit (ISCO).

Our relativistic disk model assumes a thermal electron distribution function, neglects thermal conduction, and assumes a constant ratio of ion to electron temperature T_i/T_e . The model does not produce the observed IR flaring at the correct amplitude, but can with the addition of a small nonthermal component in the distribution function (Leung 2010). If we fix the black hole mass ($M_{BH} = 4.5 \times 10^6 M_\odot$, Ghez et al. 2008) and distance ($D = 8.4$ kpc, Gillessen et al. 2008), the remaining model parameters are the source inclination i , black hole spin a_* ($0 \leq a_* \leq 1$), T_i/T_e , and \dot{M} . We fix \dot{M} so that the 1.3mm flux matches the observed $\simeq 3$ Jy.

The relativistic accretion models are not tightly constrained by the data, but they reveal the following: (1) face-on models that reproduce the millimeter flux would look like rings and therefore, in VLBI data, have dips in visibilities on fixed intermediate baselines, while existing observations suggest that the ring radius would need to vary to fit the data (Fish et al. 2011; see also the discussion of Broderick et al. 2011). More nearly edge-on models are therefore favored; (2) models with $a_* \gtrsim 0.98$ that reproduce the millimeter flux have a hot, dense inner disk that would overproduce X-rays via inverse Compton scattering. Lower spin, $a_* \sim 0.9$, models are therefore favored; (3) the observed source size and flux fix the temperature of the emitting electrons $T_e = F_\nu c^2 / (4\pi k \nu^2 \sigma^2)$ ($\sigma \equiv$ the RMS size of the source on the sky) and this turns out to favor $T_i/T_e \simeq 3$ models. The “best-bet” model from Mościbrodzka et al. (2009) has $a_* \simeq 0.94$, $i = 85$ deg, $\dot{M} \equiv \dot{M}_0 \simeq 2 \times 10^{-9} M_\odot \text{yr}^{-1}$, and $T_i/T_e = 3$.

The relativistic disk model uses self-consistent dynamics and radiative transfer but is not unique. The electron distribution function is particularly poorly constrained. It is likely anisotropic, may contain multiple temperature components (Riquelme et al. 2012) and power-law components, and vary in basic functional form with time and position. Alternative accretion models (e.g. Broderick et al. 2011, Shcherbakov et al. 2010) make different assumptions about the flow and/or distribution function and favor slightly different \dot{M} , a_* , and i . These models may respond differently to an increase in \dot{M} .

Indeed, radically different models may also fit the data. The model dynamics depends on the initial magnetic field distribution, particularly the distribution of vertical flux through the accretion disk; models with large vertical magnetic flux (e.g. McKinney et al. 2012) are likely to respond quite differently to variations in the mass flux. Also, jet models for Sgr A* (Falcke & Markoff 2000, Loeb & Waxman 2007, Falcke et al. 2009) posit a luminous jet and

a comparatively dim accretion disk. Again, these may respond differently to an influx of mass.

How, then, does our relativistic disk model respond to an increase in \dot{M} ? In this *Letter* we calculate the 1.3 and 0.87mm flux and source size as well as the spectrum that would result for the best-bet model over a range of \dot{M} . One key question we seek to answer is whether a small increase in \dot{M} would hide the event horizon (and the signature ring-like appearance of the photon orbit, also known as the shadow or silhouette of the event horizon) underneath a synchrotron photosphere. This might prevent detection of the photon orbit by the planned Event Horizon Telescope (Doeleman et al. 2008). Another key question is whether the increased \dot{M} would make Sgr A* detectable in its quiescent state in the IR and X-ray. Below we describe variation of the flux and source morphology at 230GHz (1.3mm) and 345GHz (0.87mm) (§ 2), describe variation of the spectrum (§ 3), and finally discuss which features of the results are likely to be most robust (§ 4).

2. Change of Sgr A* sub-mm luminosity and size for enhanced \dot{M}

How do we naively expect the mm disk image size and flux to respond to changes in \dot{M} ? In our model, 1.3mm emission in Sgr A* is thermal synchrotron emission from plasma with optical depth $\tau_\nu \sim 1$, near the ISCO. The true electron distribution undoubtedly contains nonthermal components (see, Riquelme et al. 2012). Models with thermal + power-law distribution functions (e.g. Broderick et al. 2011) contain an O(1/3) nonthermal contribution to the flux at 1.3mm, which hints at how uncertainty in the distribution function translates into uncertainties in the spectrum.

The thermal synchrotron absorptivity is $\alpha_{\nu,a} = j_\nu/B_\nu$, where $j_\nu = \frac{\sqrt{2}\pi e^2 n_e \nu_s}{3cK_2(\Theta_e^{-1})} (X^{1/2} + 2^{11/12} X^{1/6})^2 \exp(-X^{1/3})$, $X = \nu/\nu_s$, $\nu_s = 2/9(eB/2\pi m_e c)\Theta_e^2 \sin\theta$, θ is an angle between the magnetic field vector and emitted photon, K_2 is a modified Bessel function of the second kind (Leung et al. 2011) and $B_\nu \simeq 2\nu^2\Theta_e m_e$. Near 1.3mm, $X \sim 1$, and the emissivity is nearly independent of frequency, so $j_\nu \propto \nu^0 n_e B$ and $\alpha_{\nu,a} \propto \nu^{-2} n_e B \Theta_e^{-1}$.

We will assume that $n_e \propto \dot{M} r^{-3/2}$, $\Theta_e \propto 1/r$, and $\beta \sim \text{const.}$, so that $B \propto \dot{M}^{1/2} r^{-5/4}$ for $r > GM/c^2$, and ignore relativistic corrections. Then for $\tau_\nu \ll 1$ (or $\dot{M} \ll \dot{M}_0$) the source has size $\sim GM/c^2$ and the flux $F_\nu \sim (4/3)\pi(GM/c^2)^3 j_\nu \propto \dot{M}^{3/2}$. For $\tau_\nu \gg 1$ the source size is set by the photosphere radius r_{ph} where $\int_{r_{ph}}^\infty \alpha_a(r) dr = 1$ (i.e. for $\dot{M} \gg \dot{M}_0$, but not so large that $\Theta_e(r_{ph}) < 0.5$ so that our emissivity approximation fails). Then $r_{ph} \propto \dot{M}^{3/2}/\nu^2$, and the flux $F_\nu \propto r_{ph}^2 B_\nu(r_{ph}) \sim \dot{M}^{9/4}/\nu$.

These simple scaling laws, unfortunately, are not a good description of the variation of

source size and flux with \dot{M} . There are at least three reasons for this. First, relativistic effects are very important; for $\dot{M} \sim \dot{M}_0$ emission comes from close to the photon orbit and the source size is determined by Doppler beaming and gravitational lensing. Second, for the best-bet model at 1.3mm $\tau_\nu \sim 1$, so in a turbulent flow there is a complicated variation of the size of the effective photosphere with \dot{M} . Third, the emissivity is not precisely frequency independent near peak. We therefore need to turn to numerical models.

The best-best model is taken from a survey of 2D models. Here we adopt the best-bet model parameters ($a_* = 0.94$, $i = 85$ deg and $T_i/T_e = 3$) and use them to set parameters for a fully 3D model (Shiokawa et al. 2011)¹. We use the same data set as Dolence et al. (2012), and choose three representative snapshots taken at times when the flow is quiescent ($t = 5000, 9000$ and $13000 GM/c^3$, where $GM/c^3 = 20$ s). We then recalculate disk images and spectra for $\dot{M} = (0.5, 1, 2, 4, 8, 16, 32, 64)\dot{M}_0$.

The 3D model with $\dot{M} = \dot{M}_0$ is broadly consistent with observational data but is slightly more luminous at higher energies than 2D models (β is lower in the 3D models, and this changes the X-ray to millimeter color). The model is self-consistent only for $\dot{M} < 64\dot{M}_0$. At higher \dot{M} the efficiency of the flow is > 0.1 and therefore our neglect of cooling in the underlying GRMHD model is not justified. At higher \dot{M} the 1.3mm photosphere also lies outside the limited range in radius where $\langle d\dot{M}/dr \rangle = 0$, so the flow is not in a steady state.

The images and total fluxes emitted by the disk at 230 and 345GHz are calculated using a ray tracing scheme (Noble et al. 2007). To estimate the size of the emitting region we calculate the eigenvalues of the matrix formed by taking the second angular moments of the image on the sky (the principal axis lengths). The major and minor axis eigenvalues, σ_1 and σ_2 respectively, are related by $\sigma = \text{FWHM}/2.3$ to the FWHM of the axisymmetric Gaussian model used to interpret the VLBI observations. We use $\langle \sigma \rangle = (\sigma_1 + \sigma_2)/2$ to measure the average radius of the emitting spot.

Figures 1 and 2 show the variation of 230 and 345 GHz Sgr A* model images with \dot{M} (based on a single snapshot from the 3D GRMHD simulation). Evidently modest increases \dot{M} will make the ring-like feature that is the observational signature of the photon orbit easier to detect. For $\dot{M} \gtrsim 8\dot{M}_0$, however, the ring (or black hole silhouette) is hidden beneath the synchrotron photosphere at 230 GHz. The silhouette survives for higher \dot{M} at 345 GHz, disappearing only at $\dot{M} \gtrsim 16\dot{M}_0$. For low \dot{M} the silhouette is also difficult to detect because the emitting region is too small.

¹A 3D GRMHD model parameter survey is still too computationally expensive. It also has a poor return on investment given the electron distribution function uncertainties.

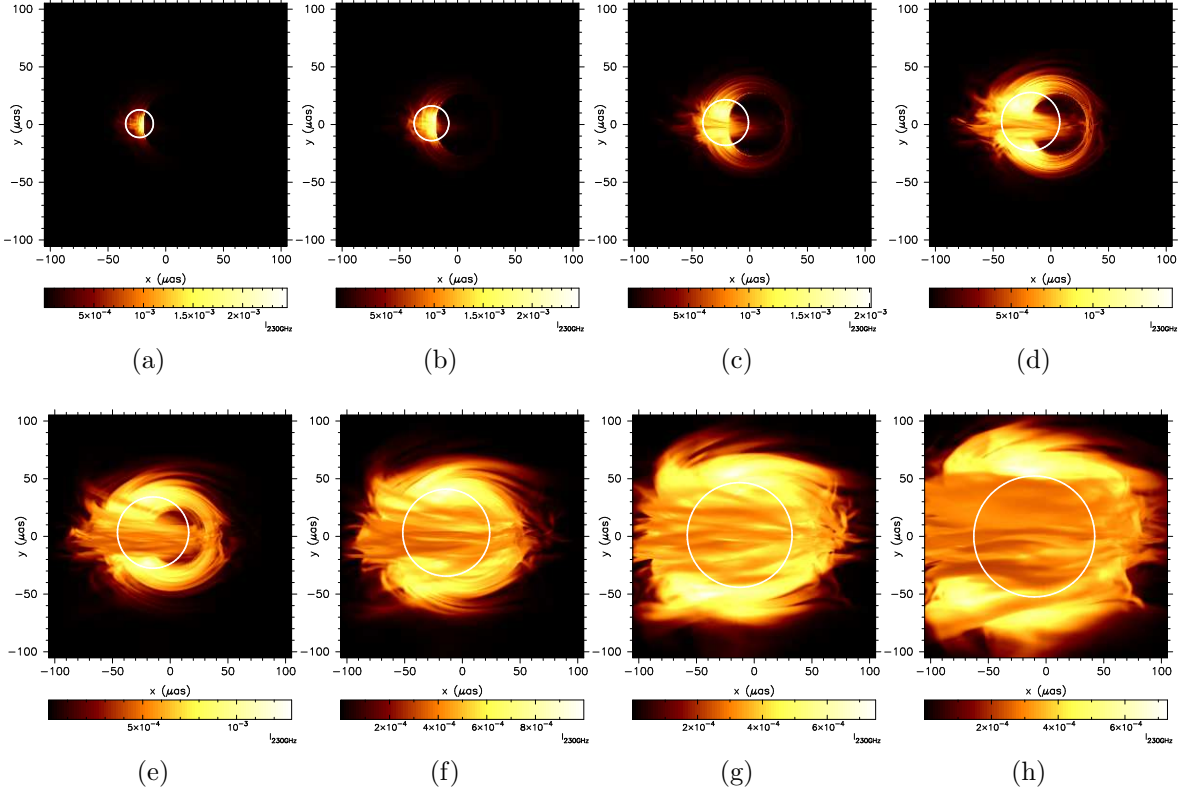


Fig. 1.—: Horizon silhouette detectability at 230 GHz for various \dot{M} . Panels from a) to h) show the images of Sgr A* calculated for $\dot{M} = (0.5, 1, 2, 4, 8, 16, 32, 64)\dot{M}_0$, respectively. The center of the circle is positioned at the image centroid and its radius, $r = (\sigma_1 + \sigma_2)/2$ is the RMS radius of the emitting region.

Figure 3, shows the accretion flow image size ($\langle\sigma\rangle$, circle radii in Figure 1 and 2) and flux at 230 and 345GHz as a function of \dot{M} . Different point types correspond to three different snapshots from the 3D GRMHD simulation. The size of the emission region and flux increase with \dot{M} . The 345/230 GHz flux ratio increases with the increasing \dot{M} ; this is caused by the shift of the synchrotron peak towards higher energies at higher \dot{M} .

The following simple fitting formulas describe how σ and F_ν depend on \dot{M} :

$$\langle\sigma\rangle_{230\text{GHz}} = \begin{cases} 15.2 \times \left(\frac{\dot{M}}{M_0}\right)^{0.38}, & \text{for } \frac{\dot{M}}{M_0} < 2 \\ 21.1 \times \log_{10}\left(\frac{\dot{M}}{M_0}\right) + 13, & \text{for } \frac{\dot{M}}{M_0} \geq 2 \end{cases} \quad [\mu\text{as}] \quad (1)$$

$$\langle\sigma\rangle_{345\text{GHz}} = \begin{cases} 12 \times \left(\frac{\dot{M}}{M_0}\right)^{0.31}, & \text{for } \frac{\dot{M}}{M_0} < 2 \\ 19.7 \times \log_{10}\left(\frac{\dot{M}}{M_0}\right) + 8.3, & \text{for } \frac{\dot{M}}{M_0} \geq 2 \end{cases} \quad [\mu\text{as}] \quad (2)$$

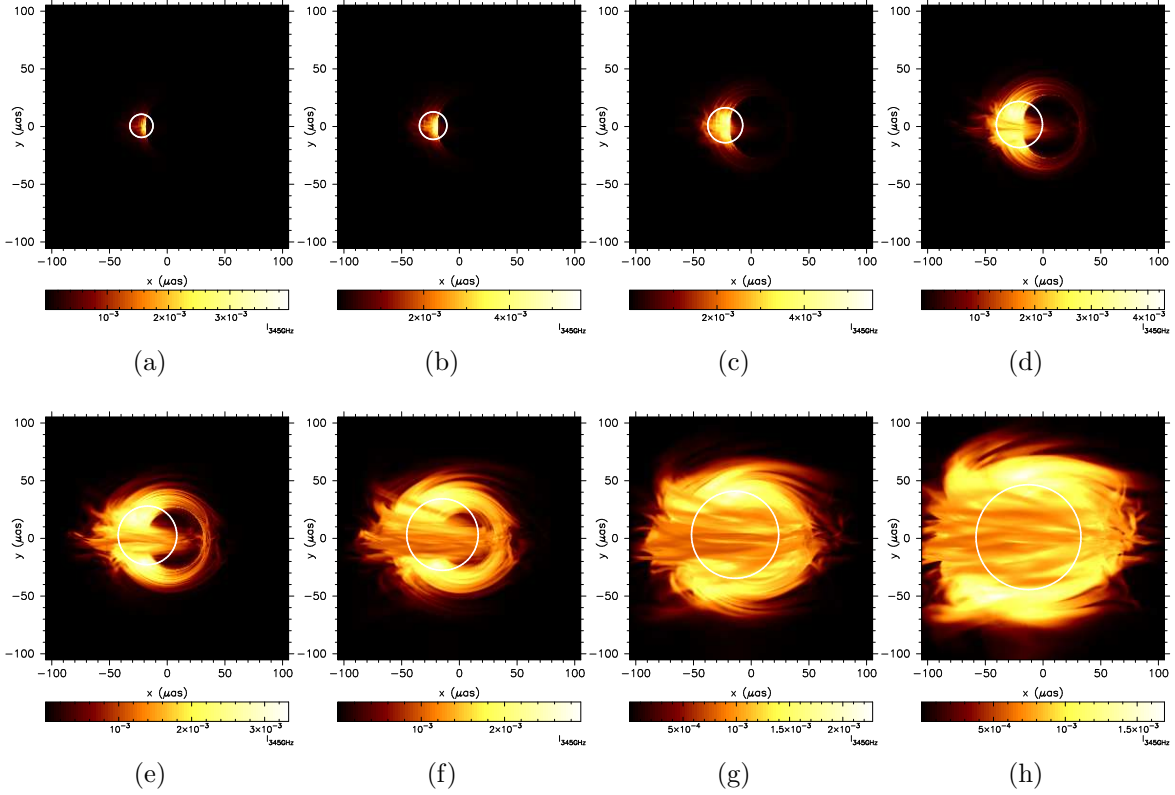


Fig. 2.—: Same as in Figure 1 but for $\nu = 345$ GHz.

$$F_{230\text{GHz}} = \begin{cases} 3.17 \times \left(\frac{\dot{M}}{M_0}\right)^{1.03}, & \text{for } \frac{\dot{M}}{M_0} < 2 \\ 10.62 \times \log_{10}\left(\frac{\dot{M}}{M_0}\right) + 3.8, & \text{for } \frac{\dot{M}}{M_0} \geq 2 \end{cases} \text{ [Jy]} \quad (3)$$

$$F_{345\text{GHz}} = \begin{cases} 3.2 \times \left(\frac{\dot{M}}{M_0}\right)^{1.3}, & \text{for } \frac{\dot{M}}{M_0} < 2 \\ 25.13 \times \log_{10}\left(\frac{\dot{M}}{M_0}\right) + 0.54, & \text{for } \frac{\dot{M}}{M_0} \geq 2 \end{cases} \text{ [Jy]} \quad (4)$$

The above constants are nontrivial to interpret because they encapsulate the complexities of the accretion flow structure and relativistic effects in the radiation transport. The advantage of the above formulas is their simplicity. The fitting functions are shown in Figure 3 as dashed and dotted lines.

Figure 4 shows the relation between two observables, σ and F_ν . The size is a linear function of the flux and increases more steeply at 230 GHz than at 345 GHz. We also provide two phenomenological scaling laws fitted to the data:

$$\langle \sigma \rangle_{230\text{GHz}} = 1.72(F_{230\text{GHz}}/\text{Jy}) + 9.3 \text{ [\mu as]} \quad (5)$$

$$\langle \sigma \rangle_{345\text{GHz}} = 0.73(F_{345\text{GHz}}/\text{Jy}) + 9.2 \text{ [\mu as]} \quad (6)$$

Notice that these fits apply to the best-bet model only. For other a_* , T_i/T_e , or i the scalings will be slightly different, although if the source is optically thick the linear scaling follows directly from $T_e \propto 1/r$.

Notice that Equation 5 predicts the change of Sgr A* size by 9 per cent when 230 GHz flux changes from 2 to 2.7 Jy. Taking into account observational and theoretical uncertainties this is consistent with the observed variations of the size of the source which increases by a few per cent as the flux increases from 2 to 2.7 Jy (Fish et al. 2011).

3. Spectra

Our model spectra are generated by thermal synchrotron emission in the submillimeter/far-IR bump, and by Compton scattering in the X-rays. The spectral slope of flaring NIR emission, and its high degree of linear polarization (Dodds-Eden et al. 2011), imply that it is synchrotron from a small, nonthermal tail of high energy electrons that is not (but can be; see Leung 2010) included in our best-bet model.

What are the expected scaling laws? Again, $j_\nu \sim n_e B \sim \dot{M}^{3/2}$. The luminosity around the synchrotron peak is $L_{peak} \sim 4\pi\nu_{peak} j_{\nu_{peak}} (GM/c^2)^3 \sim \dot{M}^{9/4}$, where $\nu_{peak} \sim \dot{M}^{3/4}$ is such that $\alpha_\nu GM/c^2 = 1$.

The emission rightward of the MIR/NIR is produced by Compton up-scattered synchrotron radiation. The Thomson depth $\tau_{sc} = \sigma_{TH} n_e GM/c^2 \sim \dot{M}$, the X-ray luminosity is expected to scale as: $\nu L_\nu(\nu \approx 10^{18}\text{Hz}) \sim L_{peak} \tau_{sc} \sim \dot{M}^{13/4}$, assuming that X-rays are produced primarily by singly scattered synchrotron photons.

What do the numerical models show? Figure 5 shows spectra emitted from the 3D disk model as observed at $i \approx 85$ deg. The SEDs are calculated using a general relativistic Monte Carlo scheme (Dolence et al. 2009). The NIR luminosity $\nu L_\nu(\nu = 10^{14}\text{Hz}) \sim \dot{M}^{2.5}$, which is only slightly steeper than the expected dependence for the synchrotron peak. $\nu L_\nu(\nu \approx 10^{18}\text{Hz}) \sim \dot{M}^{3.25}$ agrees well with the expected scaling.

We conclude that Sgr A* would become a persistent MIR and X-ray source (above the present upper limits of 84mJy in MIR and $2.4 \times 10^{33}\text{ergs}^{-1}$ in X-rays) if $\dot{M} > 2\dot{M}_0$. This is conservative in the sense that our models are strictly thermal. The addition of a high energy nonthermal tail would only increase the MIR/NIR and X-ray flux.

We do not consider higher accretion rate models because for $\dot{M} = 64\dot{M}_0$ ($\nu L_\nu(\nu = 10^{18}\text{Hz}) = 10^{39}\text{ergs}^{-1}$) the model becomes radiatively efficient, $\epsilon = L_{Bol}/\dot{M}c^2 > 0.1$, and our

neglect of radiative cooling in the underlying 3D GRMHD model is unjustified.

Finally, notice that the MeV flux increases sharply with \dot{M} . This suggests that electron-positron pair production by photon-photon collisions in the funnel over the poles of the hole would increase sharply (the pair production $\dot{n}_{e\pm} \sim L_\gamma^2$, Mościbrodzka et al. 2011). If this pair production is connected to jet production, it is reasonable to think that a high \dot{M} Sgr A* might also produce a jet.

4. Discussion

In summary, we have used general relativistic disk models and relativistic radiative transfer to recalculate millimeter images and spectra for Sgr A* at a range of $\dot{M} > \dot{M}_0$. Our models predict the following: (1) if the 230 GHz flux increases by more than a factor of 2, corresponding to an increase of \dot{M} by more than a factor of 2, the central accretion flow will become a persistent, detectable, MIR and X-ray source; (2) the photon orbit, which produces the narrow ring of emission visible in Figures 1 and 2, becomes easier to detect for modest increases in the 230 GHz flux; (3) the photon orbit is cloaked beneath the synchrotron photosphere at 230 GHz for $\dot{M} \gtrsim 8\dot{M}_0$, or 230 GHz flux $\gtrsim 13$ Jy; (4) the photon orbit is cloaked at 345 GHz only at higher $\dot{M} \gtrsim 16\dot{M}_0$, or 230 GHz flux $\gtrsim 17$ Jy; (5) the size of the source increases in proportion to the flux at both 230 and 345 GHz. We suspect that almost any accretion model for Sgr A* with a spatially uniform model for the plasma distribution function will reach qualitatively similar conclusions, but that jet models may differ significantly. There are order-unity uncertainties in our model predictions due to uncertainties in the plasma model.

What range of changes in \dot{M} are reasonable? In our best-bet model the mass at radii within a factor of two of the pericenter radius is $\approx 10^{-2.5} M_\oplus$, assuming steady mass inflow from r_p to the event horizon. The addition of even a fraction of the inferred cloud mass to the accretion flow in a ring near r_p would (eventually) increase \dot{M} by a factor of ~ 300 . On the other hand, stellar winds supply mass in the neighborhood of the central black hole at $\sim 10^{-3} M_\odot yr^{-1}$. Models by Quataert (2004) and Shcherbakov & Baganoff (2010) suggest that most of this mass is ejected in the form of a wind, and that $\sim 10^{-4.5} M_\odot yr^{-1}$ to $10^{-7.3} M_\odot yr^{-1}$ flows inward. A reasonable extrapolation of these models suggest the accretion flow at $r < r_p$ has a mass of $\sim 2M_\oplus$; this is comparable to estimates of the mass of the inflowing cloud, so in this case we might expect a factor of 2 increase in \dot{M} .

This work was supported by the National Science Foundation under grant AST 07-09246 and by NASA under grant NNX10AD03G, through TeraGrid resources provided by NCSA

and TACC.

REFERENCES

- An, T., Goss, W. M., Zhao, J.-H., Hong, X. Y., Roy, S., Rao, A. P., & Shen, Z.-Q. 2005, *ApJ*, 634, L49
- Baganoff, F. K., Bautz, M. W., Brandt, W. N., Chartas, G., Feigelson, E. D., Garmire, G. P., Maeda, Y., Morris, M., Ricker, G. R., Townsley, L. K., & Walter, F. 2001, *Nature*, 413, 45
- Baganoff, F. K., Maeda, Y., Morris, M., Bautz, M. W., Brandt, W. N., Cui, W., Doty, J. P., Feigelson, E. D., Garmire, G. P., Pravdo, S. H., Ricker, G. R., & Townsley, L. K. 2003, *ApJ*, 591, 891
- Bower, G. C., Falcke, H., Wright, M. C., & Backer, D. C. 2005, *ApJ*, 618, L29
- Broderick, A. E., Fish, V. L., Doeleman, S. S., & Loeb, A. 2011, *ApJ*, 735, 110
- Dodds-Eden, K., Gillessen, S., Fritz, T. K., Eisenhauer, F., Trippe, S., Genzel, R., Ott, T., Bartko, H., Pfuhl, O., Bower, G., Goldwurm, A., Porquet, D., Trap, G., & Yusef-Zadeh, F. 2011, *ApJ*, 728, 37
- Doeleman, S. S., Weintroub, J., Rogers, A. E. E., Plambeck, R., Freund, R., & et al. 2008, *Nature*, 455, 78
- Dolence, J. C., Gammie, C. F., Mościbrodzka, M., & Leung, P. K. 2009, *ApJS*, 184, 387
- Dolence, J. C., Gammie, C. F., Shiokawa, H., & Noble, S. C. 2012, *ApJ*, 746, L10
- Falcke, H., Goss, W. M., Matsuo, H., Teuben, P., Zhao, J.-H., & Zylka, R. 1998, *ApJ*, 499, 731
- Falcke, H. & Markoff, S. 2000, *A&A*, 362, 113
- Falcke, H., Markoff, S., & Bower, G. C. 2009, ArXiv e-prints
- Fish, V. L., Doeleman, S. S., Beaudoin, C., Blundell, R., Bolin, D. E., & et al. 2011, *ApJ*, 727, L36
- Gammie, C. F., McKinney, J. C., & Tóth, G. 2003, *ApJ*, 589, 444

- Genzel, R., Schödel, R., Ott, T., Eckart, A., Alexander, T., Lacombe, F., Rouan, D., & Aschenbach, B. 2003, *Nature*, 425, 934
- Ghez, A. M., Salim, S., Weinberg, N. N., Lu, J. R., Do, T., Dunn, J. K., Matthews, K., Morris, M. R., Yelda, S., Becklin, E. E., Kremenek, T., Milosavljevic, M., & Naiman, J. 2008, *ApJ*, 689, 1044
- Gillessen, S., Eisenhauer, F., Trippe, S., Alexander, T., Genzel, R., Martins, F., & Ott, T. 2008, *ArXiv e-prints*
- Gillessen, S., Genzel, R., Fritz, T. K., Quataert, E., Alig, C., Burkert, A., Cuadra, J., Eisenhauer, F., Pfuhl, O., Dodds-Eden, K., Gammie, C. F., & Ott, T. 2012, *Nature*, 481, 51
- Leung, P. K. 2010, PhD thesis, University of Illinois
- Leung, P. K., Gammie, C. F., & Noble, S. C. 2011, *ApJ*, 737, 21
- Loeb, A. & Waxman, E. 2007, *Journal of Cosmology and Astro-Particle Physics*, 3, 11
- Marrone, D. P. 2006, PhD thesis, Harvard University
- Marrone, D. P., Moran, J. M., Zhao, J.-H., & Rao, R. 2006, *Journal of Physics Conference Series*, 54, 354
- McKinney, J. C., Tchekhovskoy, A., & Blandford, R. D. 2012, *ArXiv e-prints*
- Melia, F. & Falcke, H. 2001, *ARA&A*, 39, 309
- Mościbrodzka, M., Gammie, C. F., Dolence, J. C., & Shiokawa, H. 2011, *ApJ*, 735, 9
- Mościbrodzka, M., Gammie, C. F., Dolence, J. C., Shiokawa, H., & Leung, P. K. 2009, *ApJ*, 706, 497
- Noble, S. C., Gammie, C. F., McKinney, J. C., & Del Zanna, L. 2006, *ApJ*, 641, 626
- Noble, S. C., Leung, P. K., Gammie, C. F., & Book, L. G. 2007, *Classical and Quantum Gravity*, 24, 259
- Özel, F., Psaltis, D., & Narayan, R. 2000, *ApJ*, 541, 234
- Quataert, E. 2004, *ApJ*, 613, 322
- Riquelme, M. A., Quataert, E., Sharma, P., & Spitkovsky, A. 2012, *ArXiv e-prints*

Schödel, R., Morris, M. R., Muzic, K., Alberdi, A., Meyer, L., Eckart, A., & Gezari, D. Y. 2011, *A&A*, 532, A83

Shcherbakov, R. V. & Baganoff, F. K. 2010, *ApJ*, 716, 504

Shcherbakov, R. V., Penna, R. F., & McKinney, J. C. 2010, ArXiv e-prints

Shiokawa, H., Dolence, J. C., Gammie, C. F., & Noble, S. C. 2011, ArXiv e-prints

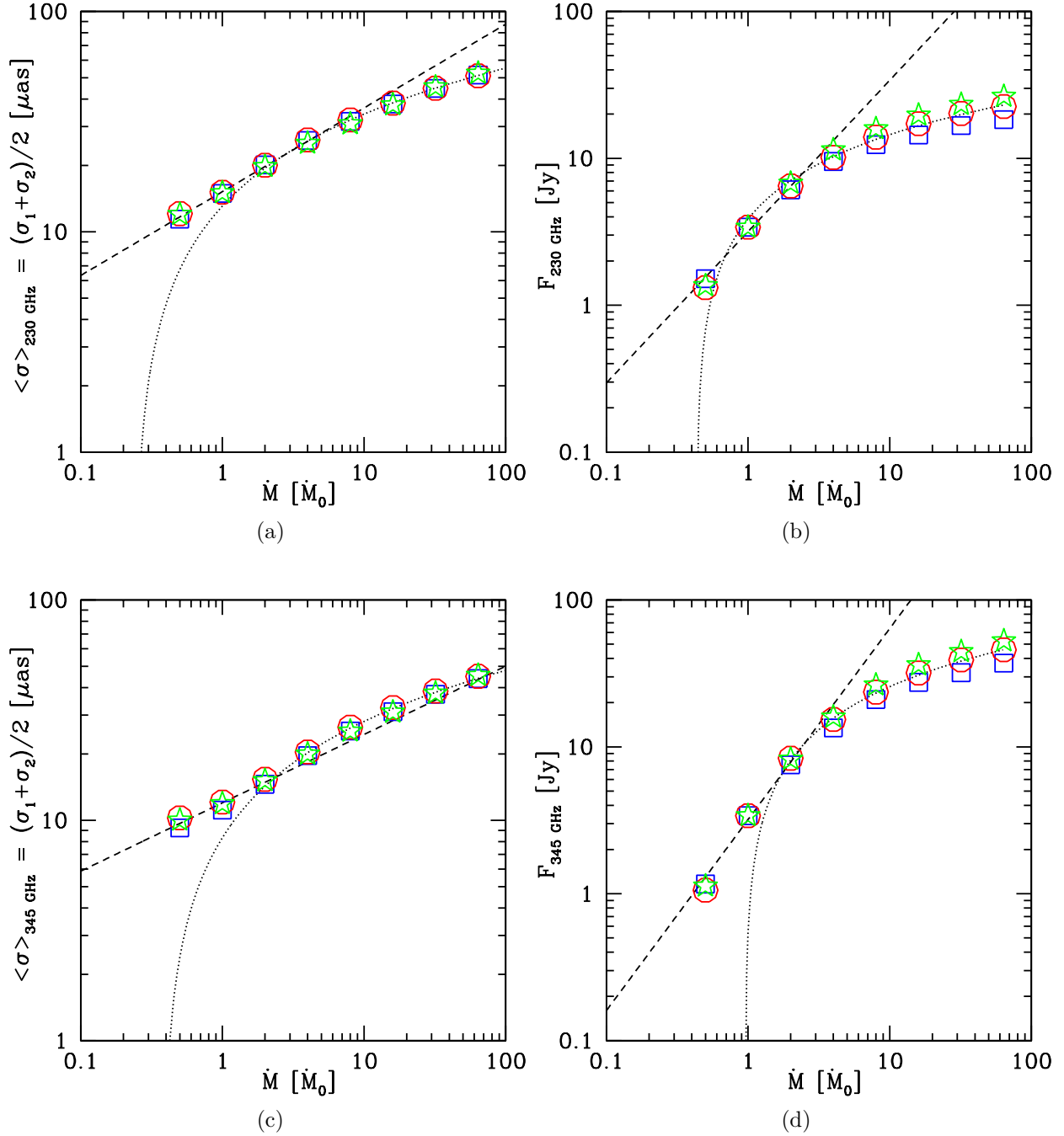


Fig. 3.—: Sizes (in terms of σ) of the emitting region and the total flux as a function of \dot{M} at 230 (upper panels) and 345GHz (lower panels). Different point types correspond to three different snapshots from the 3D GRMHD simulation. The dashed/dotted lines show the best fit to the data by Equations 1, 2, 3, and 4.

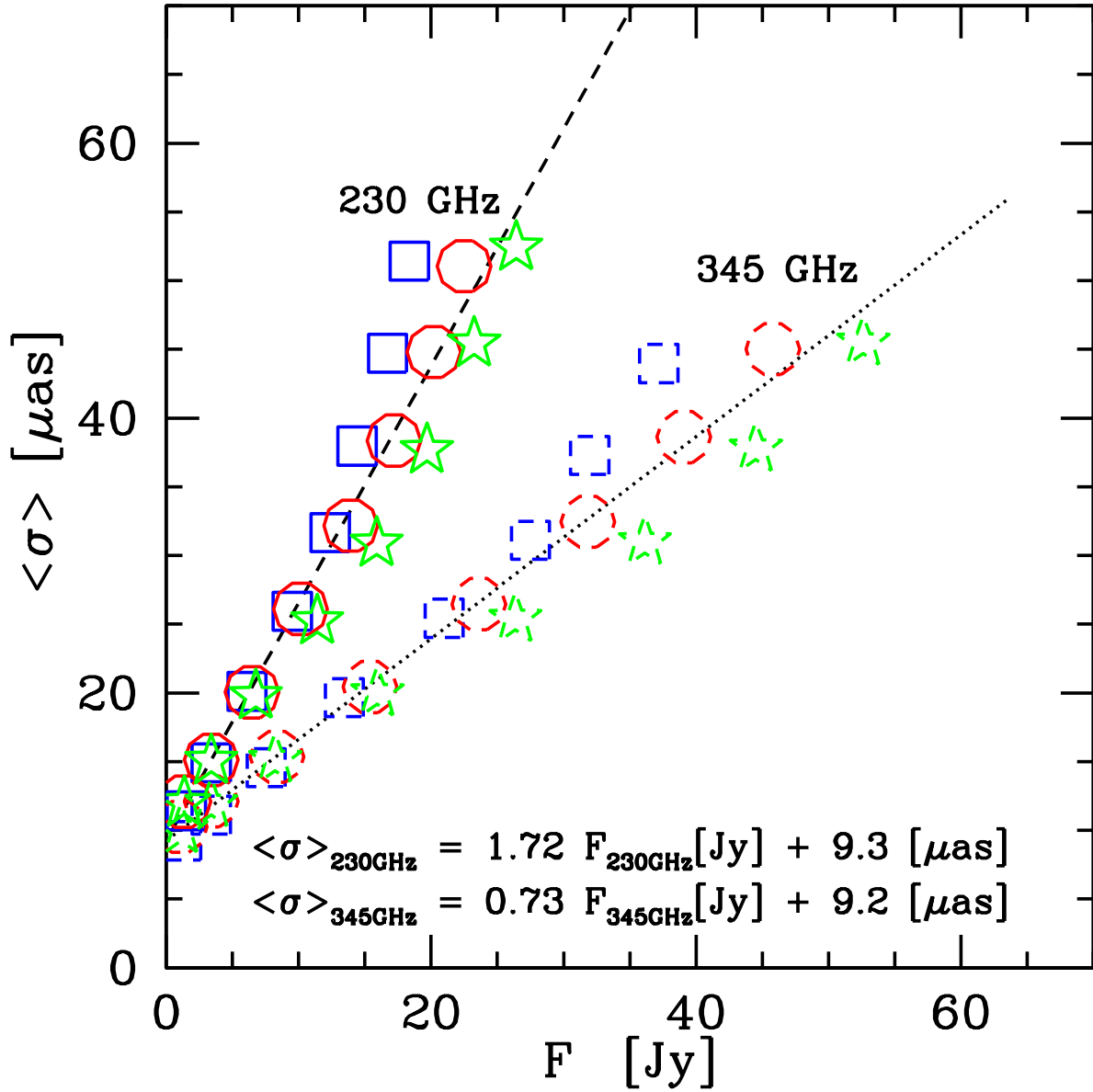


Fig. 4.—: Relation between two observables: the flux and the size of the image at $\nu = 230$ and 345 GHz. The dashed and dotted lines are the best fits to the data points.

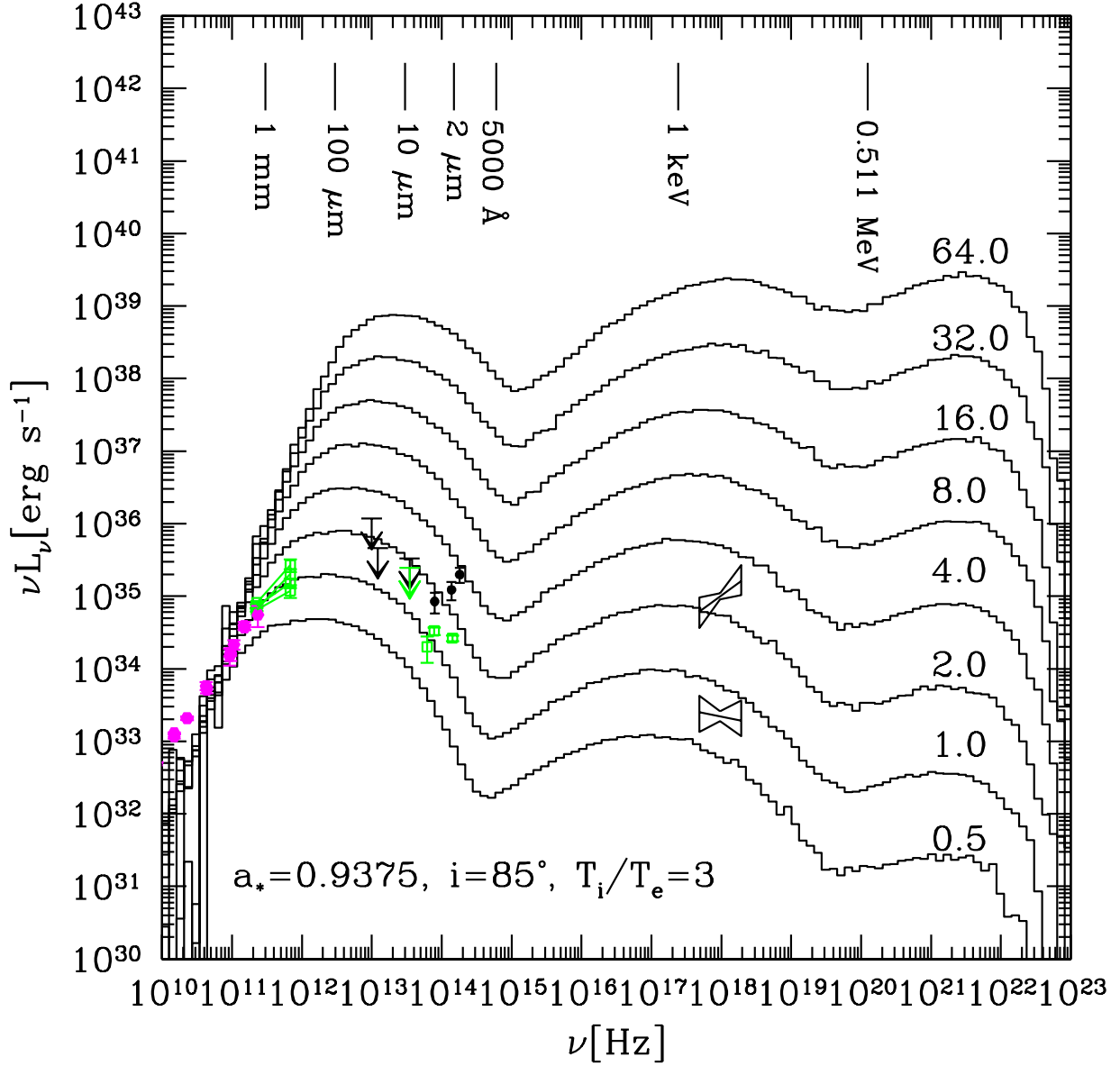


Fig. 5.—: Spectrum emitted by 3D disk model for various \dot{M} . The \dot{M}/\dot{M}_0 is shown on the righthand side. Observational points and upper limits are taken from: Falcke et al. 1998, An et al. 2005, Marrone et al. 2006, Melia & Falcke 2001, Schödel et al. 2011, Baganoff et al. 2003. The black symbols in the NIR showing the flaring state are from Genzel et al. 2003. An example of X-ray flare is taken from Baganoff et al. 2001.